Journal of Alloys and Compounds 489 (2010) 281–288

Contents lists available at ScienceDirect

Journal of Alloys and Compounds

journal homepage: www.elsevier.com/locate/jallcom

Structure, dielectric and optical properties of Nd^{3+}-doped $LiTaO_3$ transparent ferroelectric glass–ceramic nanocomposites

Anal Tarafder[a], Kalyandurg Annapurna[a], Reenamoni Saikia Chaliha[a], Vidya Sagar Tiwari[b], Pradeep Kumar Gupta[b], Basudeb Karmakar[a,*]

[a] Glass Technology Laboratory, Glass Division, Central Glass and Ceramic Research Institute (CSIR), 196, Raja S.C. Mullick Road, Kolkata 700032, India
[b] Laser Materials Development and Devices Division, Raja Ramanna Center for Advanced Technology, Indore 452013, India

ARTICLE INFO

Article history:
Received 18 August 2009
Received in revised form
14 September 2009
Accepted 15 September 2009
Available online 23 September 2009

PACS:
42.70.Ce
42.70.Mp
77.84.Dy
78.20.−e
78.55.−m
78.55.Qr

Keywords:
Transparent glass–ceramic
Ferroelectric Nd^{3+}:$LiTaO_3$ nanocrystals
Photoluminescence
Lifetime
Concentration quenching
Dielectric constant

ABSTRACT

Here, we present the structural, dielectric and optical properties of neodymium ion (Nd^{3+}) doped novel transparent glass-ceramics containing $LiTaO_3$ nanocrystals in the Li_2O–Ta_2O_5–SiO_2–Al_2O_3 (LTSA) glass system prepared by the melt-quenching technique. The precursor glasses were isothermally crystallized at 680 °C for 3–100 h, following the differential thermal analysis (DTA) data, to obtain nanostructured glass-ceramics. They were characterized by X-ray diffraction (XRD), field emission scanning electron microscope (FESEM), transmission electron microscopy (TEM), Fourier transform infrared reflection spectra (FTIRRS), optical absorption and luminescence spectroscopy along with dielectric constant measurements. XRD, FESEM, TEM and FTIRRS confirm the nanocrystallization of $LiTaO_3$ (14–36 nm) in the LTSA glass matrix. A steep increase in dielectric constant (ε_r) of glass-ceramics with heat-treatment time is observed due to high dielectric constant ferroelectric $LiTaO_3$ formation. The measured NIR photoluminescence spectra have exhibited emission transitions of $^4F_{3/2} \rightarrow {}^4I_J$ (J = 9/2, 11/2 and 13/2) from Nd^{3+} ions upon excitation at 809 nm. It is observed that the photoluminescent intensity and excited state ($^4F_{3/2}$) lifetime of Nd^{3+} ions decrease with increase in heat-treatment time due to concentration quenching effect. The absorption spectra and fluorescence measurements reveal that the incorporation of Nd^{3+} ions in the $LiTaO_3$ crystal lattice in the oxide glassy matrix is important for obtaining desirable fluorescence performance of the material.

1. Introduction

Lithium tantalate ($LiTaO_3$, LT) single crystal is one of the most important lead-free ferroelectric materials in the $A^{1+}B^{5+}O_3$ type perovskite family rhombohedral crystal structure with crystal symmetry class $R3c$ (unit cell dimensions: a = 5.1530 Å and c = 13.755 Å), having large nonlinear constant (d_{33} = 13.6 pm/V at 1064 nm) and second harmonic generation (SHG) coefficient ($d_{33}^{2w} = 40.0$ with respect to KDP at 1060 nm) [1–3]. Due to its above mentioned extraordinary optical properties, its single crystal exhibits unique piezoelectric, acousto-optic, electro-optic and nonlinear optical (NLO) properties combined with good mechanical and chemical stability [4–6]. Thus, correlation of property alteration of LT single crystals, powders, thin films, glass-ceramics, etc. with processing parameters is an important area of exploration. Consequently, in recent times researchers have demonstrated the property monitoring based on preparation of $LiTaO_3$ powders [7] and thin films [8,9] by different methods. Luminescence properties of Ho^{3+}, Eu^{3+}, Tb^{3+} etc. doped $LiTaO_3$ crystals, another important area of exploration, which have also been investigated by various researchers [10–13]. Rare-earth (RE) doped transparent $LiTaO_3$ nanocrystallite containing glass-ceramics, in which rare-earth ions selectively incorporated into the $LiTaO_3$ nanocrystals embedded in an oxide glassy matrix, can offer excellent luminescent properties due to the low phonon energy environment of $LiTaO_3$ nanocrystallites for luminescent ions, and good mechanical and chemical properties of oxide glassy matrix. This ability, combined with inherent nonlinear optical properties of ferroelectric crystals, could offer a possibility to design self frequency doubling laser sources. Hence, this new material has attracted great attention in the continuous research for the development of novel optoelectronic devices [14–18]. Mukherjee and Varma have reported the crystallization and physical properties of $LiTaO_3$ in a $LiBO_2$–Ta_2O_5 reactive glass matrix,

* Corresponding author. Tel.: +91 33 2473 3469; fax: +91 33 2473 0957.
E-mail address: basudebk@cgcri.res.in (B. Karmakar).

0925-8388/$ – see front matter © 2009 Elsevier B.V. All rights reserved.
doi:10.1016/j.jallcom.2009.09.071

however, they have not explored RE doped $LiTaO_3$ containing glass-ceramics [19]. As such, work performed on nanocrystalline $LiTaO_3$ containing aluminosilicate glass–matrix materials is very rare due to the difficulties in preparation of transparent precursor glass in general and glass-ceramics in particular which involves high temperature (about 1600 °C) for its precursor glass melting [20]. Probably for this reason, the dielectric and fluorescence properties of Nd^{3+} ion doped transparent precursor glass and glass–ceramic composites of $LiTaO_3$ with heat-treatment time have not been reported so far. This fact has motivated us to explore this opportunity.

Glass materials are attractive hosts for rare-earth ions (RE^{3+}) because planar waveguides and optical fibers can be fabricated easily with them compared to crystalline materials. Nd^{3+} is one of the most widely studied luminescent ions, and Nd^{3+}-doped crystalline, glass and ceramics have been applied in many fields. Nd^{3+} has been extensively used as laser active ion in several hosts due to high quantum efficiency of its some emission channels either by normal fluorescence in NIR region or by upconversion/frequency doubling in green-red wavelength [21–23]. Most of the Nd^{3+} lasers operate in NIR region on two lasing transitions $^4F_{3/2} \rightarrow {}^4I_{11/2,13/2}$ at around 1060 nm and 1349 nm wavelengths respectively based on four level systems. During the past few years the $^4F_{3/2} \rightarrow {}^4I_{9/2}$ laser transition near 900 nm of the neodymium ion has also attracted much attention for its applications especially in display technologies, as it opens the way for efficient generation of continuous blue laser radiation in the watt range by means of a compact, all-solid-state frequency doubling laser [24]. The main basis for such a laser is provided by novel high-power diode-laser sources that offer high beam brightness for longitudinal pumping because the three level nature of this laser transition requires high pump intensities for efficient laser output. Apart from its high quantum efficiency performance as laser active ion, Nd^{3+} has also been well exploited as a structural probe in studying the local field effects around the dopant ions [25] as it possesses hypersensitive transitions. As we aware, there is no report on Nd^{3+}-doped transparent $LiTaO_3$ glass-ceramics prepared by controlled crystallization of melt-quench precursor glass. Hence, it will be very interesting to investigate the evolution of spectroscopic along with structural and dielectric properties of doped Nd^{3+} ions in $LiTaO_3$ glass–ceramic nanocomposites.

In view of above, in the present work we focus our systematic analysis on the precursor glass preparation, crystallization, structure and optical properties of isothermally crystallized Nd^{3+} ion doped Li_2O–Ta_2O_5–SiO_2–Al_2O_3 transparent glasses. The crystallization process has been studied by differential thermal analysis (DTA), X-ray diffraction (XRD), field emission scanning electron microscopy (FESEM), transmission electron microscopy (TEM), Fourier transform infrared reflection spectra (FTIRRS), optical absorption, NIR-excited (809 nm) NIR fluorescence and excited state lifetime.

It is obvious that the ferroelectric crystal containing glass-ceramics would have relatively high dielectric constant than its precursor glass due to the high spontaneous polarization ($P_s = 0.50\,C/m^2$ for $LiTaO_3$) as well as induced polarization of ferroelectric crystal under applied electric field [1]. Kim et al. [26] reported the dielectric properties during phase transition of the $LiTaO_3$–SiO_2 glasses produced by the twin roller quenching method. Hence, a study has also been carried out on how the dielectric properties (dielectric constant) change with progression of isothermal nanocrystallization of precursor Nd^{3+}-doped LTSA glasses.

2. Experimental procedures

The precursor glass having molar composition $25.53Li_2O$–$21.53Ta_2O_5$–$35.29SiO_2$–$17.65Al_2O_3$ doped with Nd_2O_3 (0.5 wt% in excess) was prepared from high-purity chemicals such as Li_2CO_3 (GR, 99%, Loba Chemie), Ta_2O_5 (99.85%, Alfa Aesar), SiO_2 (99.8%, Sipur A1 Bremtheler Quartzitwerk), Al_2O_3 (99.8%, CT 1200 SG, Almatis), and Nd_2O_3 (99.99%, Alfa Aesar) by conventional melt-quench technique. The well-mixed batch of about 250 g glass was melted in a platinum crucible in an electric furnace at 1600 °C for 2 h in air. The glass melt was poured onto a pre-heated iron mould. It was annealed at 600 °C for 4 h to remove the internal stresses of the glass and then slowly cooled down to room temperature. The as-prepared glass block was cut into desired dimensions and optically polished for ceramization and to performing different measurements.

The density of precursor glass was measured using Archimedes principle using water as buoyancy liquid. The refractive index of precursor glass was measured by a Prism Coupler (Model: 2010/M, Metricon Corporation) at five different wavelengths (λ = 473, 532, 633, 1064 and 1552 nm). Differential thermal analysis (DTA) of precursor glass powder was carried out up to 1000 °C from room temperature at the rate of 10 °C/min with a SETARAM instrument (Model: TG/DTA 92, SETARAM Instrumentation) to establish the glass transition temperature (T_g) and the crystallization peak temperature (T_p). XRD data were recorded using an XPERT-PRO MPD diffractometer (PANalytical) with Ni-filtered CuK_α = 1.5406 Å radiation as the X-ray source to identify the developed crystalline phases. The 2θ scan range was 10–80° with a step size of 0.05°.

A high resolution FESEM (Gemini Zeiss Supra™ 35 VP model of Carl Zeiss Microimaging GmbH) was used to observe the microstructure of freshly fractured surfaces of the heat-treated glass–ceramic nanocomposites after etching in 1% HF solution for 2 min, dried and then coated with a thin carbon film. The TEM images and selected area electron diffraction (SAED) of powdered glass–ceramic sample were obtained from FEI (Model: Tecnai G^2 30ST, FEI Company) instrument. The FTIR reflectance spectra of all Nd^{3+}-doped glass and glass-ceramics were recorded using a FTIR spectrometer (Model: 1615 Series, PerkinElmer Corporation) in the wavenumber range 400–2000 cm^{-1} with a spectral resolution of ±2 cm^{-1} and at 15° angle of incidence. Optical absorption spectra were recorded UV–vis-NIR spectrophotometer (Lambda 20, PerkinElmer Corporation) at room temperature to monitor the changes of the environmental structure of the Nd^{3+} ions. The NIR-excited (809 nm) emission spectra were measured on NIR enhanced continuous bench top modular spectrofluorimeter (QuantaMaster, Photon Technology International) attached with gated Hamamatsu NIR PMT (P1.7R) as detector and Xe arc lamp as excitation source. The excited state lifetime was measured with the same instrument using a Xe flash lamp of 75 W. The dielectric constant of glass and glass–ceramic nanocomposites was measured at room temperature using a LCR meter (Model: 3532-50 Hitester, Hioki) at 1 MHz frequency after coating the surfaces with a conductive silver paint followed by drying at 140 °C for 1 h.

3. Results and discussion

3.1. Thermal, optical and other physical properties

The DTA curve of the precursor glass is shown in Fig. 1. It exhibits an inflection in the temperature range 680–715 °C followed by a very intense exothermic peak at 820 °C (T_p) corresponding to the $LiTaO_3$ crystallization. The glass transition temperature (T_g) has been estimated to be 702 °C from the point of intersection of the tangents drawn at the slope change as marked in Fig. 1 of the DTA curve.

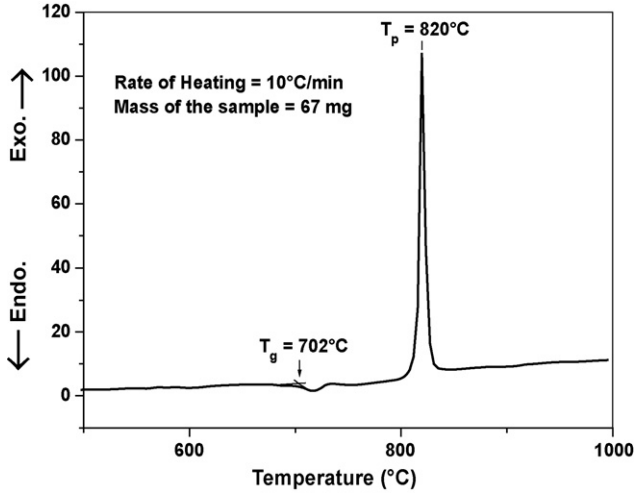

Fig. 1. DTA curve of Nd^{3+}:$LiTaO_3$ precursor glass powder.

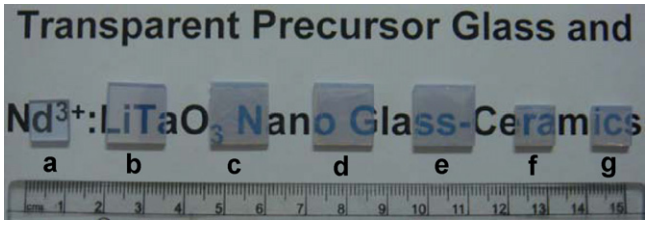

Fig. 2. Photograph of Nd^{3+}:$LiTaO_3$ precursor glass and glass–ceramic nanocomposites (thickness: 2 mm) laid over the writing to show their transparency. (For interpretation of the references to color in this figure legend, the reader is referred to the web version of the article.)

The precursor glass is visually transparent, appearing blue-purple due to Nd^{3+} doping. The precursor glass samples were heat treated at 680 °C near glass transition temperature for 0, 3, 5, 10, 20, 50 and 100 h after nucleating at 650 °C for 2 h. The obtained samples were labeled as (a)–(g) (Fig. 2) respectively for convenience. The transparency of the precursor glass persists in heat-treated samples although the samples have been appeared gradually translucent due to devitrification with progress of heat-treatment duration. Fig. 3 presents Cauchy fitting based on measured refractive indices at five different wavelengths (see Section 2) and shows the dependences of the refractive index on the wavelength for precursor glass (a) and the 10 h heat-treated glass-ceramics (d) sample. In general, refractive index decreases with increasing wavelength due to dispersion. This trend is observed in both the samples. In addition to this, the refractive index of the glass–ceramic sample (d) has increased in comparison with precursor glass (a) that can be seen in Fig. 3. The refractive indices n_F, n_D and n_C have been estimated at three standard wavelengths (λ_F = 486.1 nm, λ_D = 589.2 nm and λ_C = 656.3 nm respectively) from the dispersion curve (Fig. 3, curve (a)). From the measured glass density (ρ) and refractive index (n_D) at wavelength λ_D = 589.2 nm, other related optical properties have been determined using relevant expressions and the results are presented in Table 1. From Table 1, it is clear that the LTSA glass under study has high values of refractive index and density. The large refractive indices of this glass are due to high ionic refraction (23.4) of Ta^{5+} ions [27] having an empty or unfilled d-orbital (outer electronic configuration: $5d^0 6s^0$) which contributes strongly to the linear and nonlinear polarizability [28]. The high density of the glass has originated from the large packing effect of Ta in the glass matrix [29]. For the same reason, this glass possesses a high

Table 1
Some measured and calculated properties of Nd^{3+}:Li_2O–Ta_2O_5–SiO_2–Al_2O_3 precursor glass.

Properties	Corresponding value
Average molecular weight, M_{av}	142.37
Density, ρ (g cm^{-3})	4.50
Refractive indices	
n_F (at 486.1 nm)	1.8053
n_D (at 589.2 nm)	1.7894
n_C (at 656.3 nm)	1.7821
Abbe number (υ_D)	34
Dispersive power ($1/\upsilon_D$)	0.03
Molar refractivity, R_M (cm^3)	13.39
Electronic polarizability, α (cm^3)	1.79×10^{-21}
Nd^{3+} ion concentration, $N_{Nd^{3+}}$ (ions/cm^3)	5.66×10^{19}
Nd^{3+}–Nd^{3+} inter ionic distance, R_i (Å)	26
Glass transition temperature, T_g (°C)	702
Crystallization peak, T_p (°C)	820

value of molar refractivity (R_M = 13.39 cm^3) and electronic polarizability ($\alpha = 1.79 \times 10^{-21}$ cm^3). Due to formation of high refractive index $LiTaO_3$ (RI = 2.1834 at 600 nm [30]), the heat-treated sample exhibit higher refractive indices as shown in Fig. 3, curve (d).

3.2. X-ray diffraction analysis

The X-ray diffractograms of precursor glass and cerammed glass-ceramics are shown in Fig. 4. The XRD pattern of the precursor glass exhibits broad humps characterizing its amorphous structure. The X-ray diffraction pattern of the glass-ceramics clearly shows the structural behavior expected after a thermal treatment of the precursor glass. With progression of heat-treatment, several diffraction peaks have been appeared. From the analysis of these peaks it has been concluded that these peaks are attributed to rhombohedral $LiTaO_3$ (JCPDS Card File No. 29-0836) except a few diffraction peak around 2θ = 22.98°, 25.21°, 44.46° and 47.02° which are due to the formation of β-spodumene ($LiAlSi_2O_6$) crystal phase (JCPDS Card File No. 35-0797) in minor quantity. Hsu and Speyer [31] have reported that the Ta_2O_5 acts as a nucleating agent in the Li_2O–Al_2O_3–SiO_2 glass system which exhibits β-quartz solid solution (ss) crystallization, where β-spodumene is one of them, peak in the temperature range 800–900 °C particularly at higher concentration of Ta_2O_5. In the present case, the small crystallization peak (minor) of β-spodumene in the DTA thermogram might have

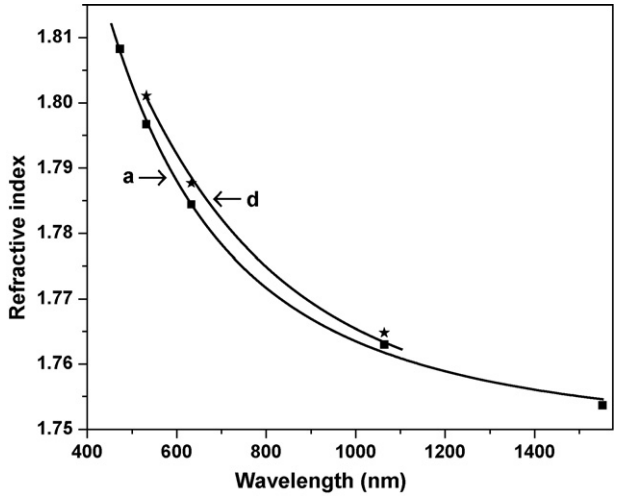

Fig. 3. Variation of refractive indices (Cauchy fitted) of Nd^{3+}:$LiTaO_3$ (a) precursor glass and (d) 10 h heat-treated glass–ceramic nanocomposites as a function of wavelength.

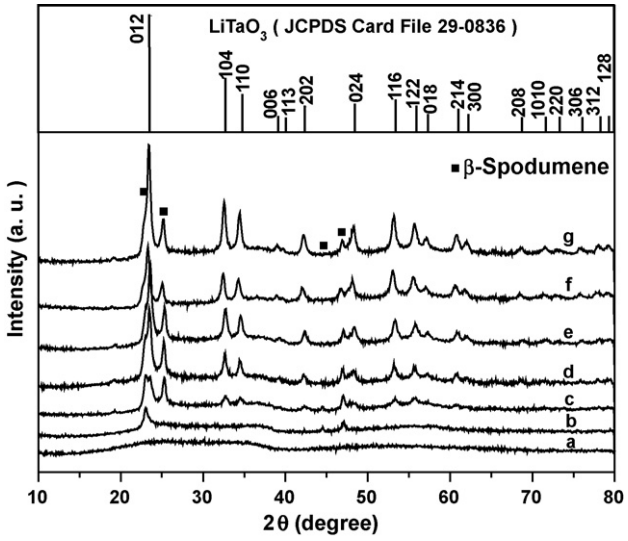

Fig. 4. XRD patterns of the samples (a)–(g).

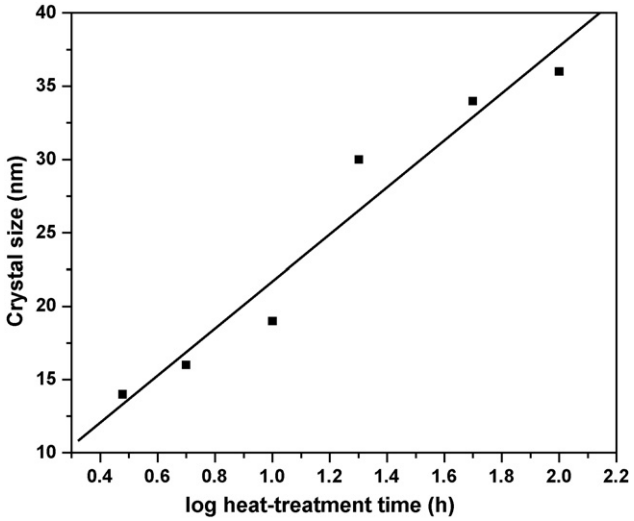

Fig. 5. Variation of crystal size as a function of heat-treatment time.

merged with the large crystallization peak (major) of the $LiTaO_3$ at 820 °C. This could be the reason of exhibiting two crystal phases in the XRD patterns although DTA curve shows only single sharp crystallization peak around 820 °C. It is clearly evidenced from the XRD analysis that the peak of $LiAlSi_2O_6$ ($2\theta = 25.21°$) is more prominent in sample (c) with 5 h heat-treatment and it got diminished with respect to $LiTaO_3$ phase in samples (d)–(g), indicating the stabilization of $LiTaO_3$ nanocrystallites with increase in heat-treatment duration. The XRD pattern of sample (b) differ due to its phase-separated glassy nature and having different structure than the precursor glass (a) and 5 h heat-treated glass–ceramic nanocomposites (c). From the full width at half maximum (FWHM) of the most intense diffraction peak (0 1 2) of $LiTaO_3$, the average crystallite size (diameter, d) is calculated by using the Scherrer's formula [32]

$$d = \frac{0.9\lambda}{\beta \cos\theta} \quad (1)$$

where λ is the wavelength of X-ray radiation ($CuK_\alpha = 1.5406$ Å), β is the full width at half maximum (FWHM) of the peak at 2θ.

The diameter of the $LiTaO_3$ crystallites is plotted as a function of heat-treatment time in Fig. 5. The average crystallite size increases with heat-treatment duration and found to vary from 14 to 36 nm for samples (b)–(g).

3.3. FESEM and TEM image analyses

The morphology and $LiTaO_3$ crystallite size in glass–ceramic nanocomposites have been examined by FESEM and TEM image analyses. FESEM images of the fractured surface of samples c and e have been presented in Fig. 6(a) and (b) respectively. From the FESEM micrographs, it is clearly observed that the glassy matrix of the heat-treated samples initially phase separated on nanometric scale followed by incipient precipitation of defined crystallites within the Li–Ta rich phase regions with increase in heat-treatment time. The droplets have irregular shapes and dispersed uniformly thought out the bulk glass matrix. The size of the droplets varies in the range 20–60 nm. The TEM bright field images and their selected area electron diffraction (SAED) patterns of the 3 and

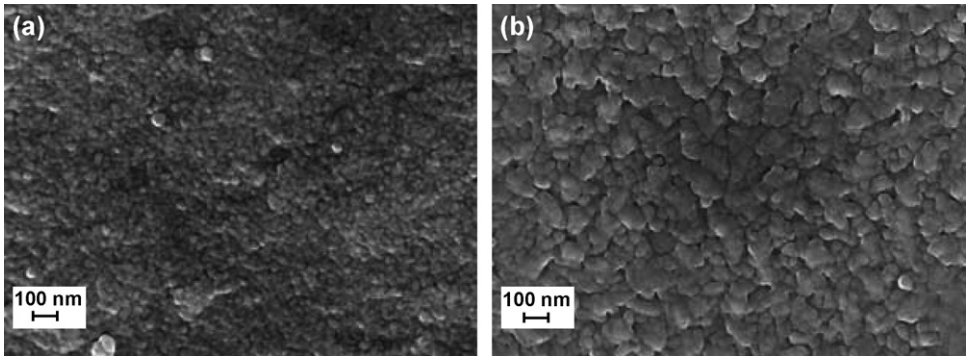

Fig. 6. FESEM images of samples (a) c and (b) e.

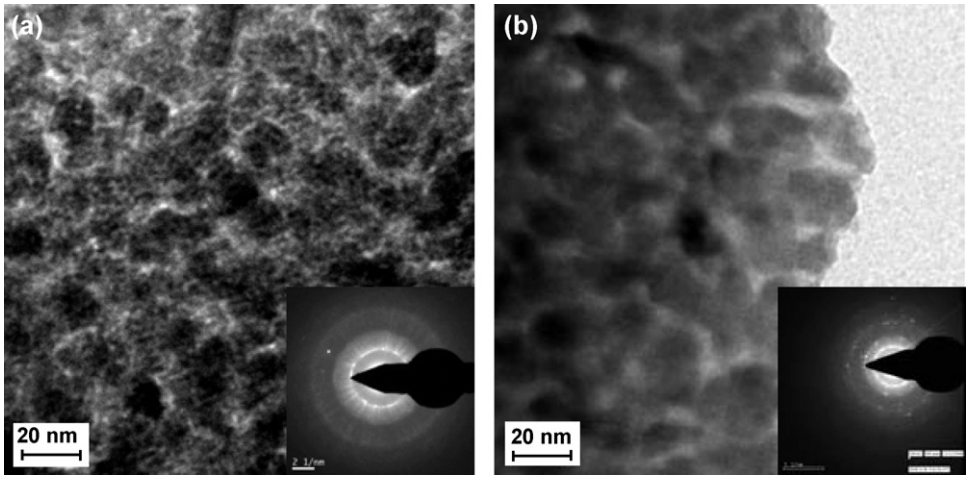

Fig. 7. (a) TEM images and SAEDs (Inset) of samples (a) b and (b) f.

50 h heat-treated samples (b) and (f) are shown in Fig. 7(a) and (b) respectively. From these images, it is observed that many spheroidal $LiTaO_3$ crystallites precipitated homogeneously from the glass matrix and remained homogeneously dispersed in the residual glass matrix. The crystallite size from TEM image of sample b is found to be around 15 nm and of sample f to be around 18 nm. The presence of fine spherical rings around the central bright region in SAED pattern discloses the existence of $LiTaO_3$ nanocrystallites in the glassy matrix.

3.4. Fourier transform infrared reflectance spectroscopy (FTIRRS)

The FTIR reflectance spectra of the as-prepared and heat-treated samples in the wavenumber range 400–2000 cm^{-1} are shown in Fig. 8. It is seen from this figure that the precursor glass (curve (a)) exhibits two broad reflection bands centered around 960 and 610 cm^{-1} as a result of wider distribution of silicon and tantalate structural units respectively. This is an indication of the existence of structural disorder in the amorphous network with the presence of SiO_4 tetrahedra and TaO_6 octahedra having different number of non-bridging oxygen. In spite of the transparent nature of the heat-treated samples, their FTIR reflectance spectra (curves (b) and (g)) reveal narrowing of two main reflection bands with additional feature arising at 735 cm^{-1} in comparison to the as-prepared glass. In the FTIRR spectra, the stretching modes of the Si–O–Si bonds of the SiO_4 tetrahedra with non-bridging oxygen (NBO) atoms are active around 1000 cm^{-1} (high energy side) and the stretching modes of the Ta–O bonds in the TaO_6 octahedra occur in the 600–650 cm^{-1} range (low energy side) due to higher atomic weight of Ta than Si. The variation of Si–O (998 cm^{-1}) and Ta–O (602 cm^{-1}) stretching vibration bands intensities (here reflectivity) with heat-treatment time is shown in the inset of Fig. 8. It is seen that with progression of heat-treatment the band intensities increase rapidly initially and then become almost saturated after a certain time of heat-treatment (10 h). The appearance of a low intensity band at 735 cm^{-1} upon heat-treatment related to the stretching mode of Al–O bond of AlO_4 tetrahedra of β-spodumene [33]. The prominent band occurred at 602 cm^{-1} corresponds to the stretching mode of Ta–O bond of TaO_6 octahedral units of lithium tantalate [34,35]. The reflection band centered at 602 cm^{-1} is assigned to $LiTaO_3$ crystal formation and the reflection band centered at 998 cm^{-1} is assigned to Si–O stretching vibration of residual glass and β-spodumene crystal. Two bands generated at 998 and 602 cm^{-1} in the FTIR spectrum (Fig. 8, curve (b)) after 3 h heat-treatment at 680 °C give the clear evidence of phase separation of precursor glass into Si-rich and Li-rich phases respectively, which exhibits very feeble sign of crystallization in the XRD pattern (Fig. 4, curve (b)). The gradual

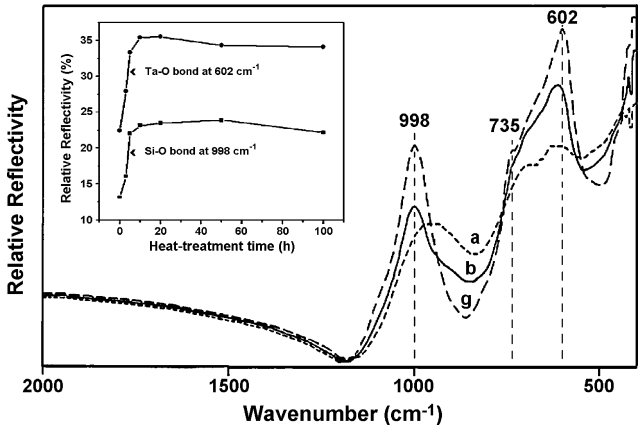

Fig. 8. FTIRR spectra of (a) precursor glass, (b) 3 h and (g) 100 h heat-treated samples.

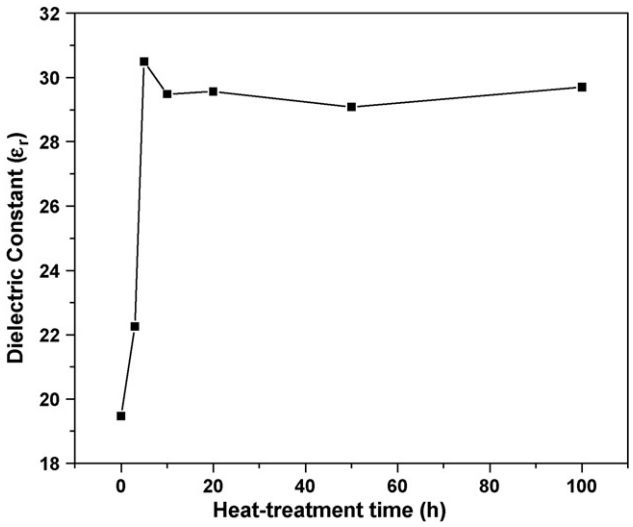

Fig. 9. Variation of dielectric constant of Nd^{3+}:$LiTaO_3$ precursor glass (a) and glass–ceramic nanocomposites ((b)–(g)) as a function of heat-treatment time.

increase of relative intensity of band at 602 cm^{-1} clearly indicates formation of $LiTaO_3$ crystal with the increase of heat-treatment time. Thus from the investigations carried out on the measured FTIR reflectance spectra of Nd^{3+}-doped Li_2O–Ta_2O_5–SiO_2–Al_2O_3 glass and glass-ceramics as described above provide the information of crystallization with initial phase separation followed by advancement of mainly $LiTaO_3$ crystal formation in the glass matrix. The results of the FTIRRS are in good agreement with that of XRD, FESEM and TEM studies. A similar observation has also been reported by Ito et al. [20].

3.5. Dielectric constant (ε_r)

Glass and glass-ceramics have certain advantages as dielectric materials because of their high dielectric strength. But the disadvantages of glass are a low permittivity (ε_r = 4–15) and a low thermal conductivity (about 1 $W m^{-1}K^{-1}$) [36]. In the present study, the as-prepared Nd^{3+}-doped Li_2O–Ta_2O_5–SiO_2–Al_2O_3 glass has exhibited relatively higher value (19.3) of dielectric constant (ε_r) than the common vitreous silica (3.8) or soda-lime silicate (7.2) or borosilicate glasses (4.1–4.9) [37] due to high ionic refraction of Ta^{5+} ions (23.4) [27]. This is due to its empty or unfilled d-orbital which contributes very strongly to its high polarizability [28,1]. Its magnitudes show a sharp increase with increase in heat-treatment duration up to 5 h and thereafter it maintained saturation with a small decrease for any further heat-treatment time as shown in Fig. 9. This suggests that, at the initial stages of heat treatment (3 h), separation of silica rich phase and Li–Ta enriched phases takes place and with the further heat-treatment, incipient precipitation of $LiTaO_3$ crystalline phase of high dielectric constant (ε_r = 52) [3] and spontaneous polarization (P_s = 0.50 C/m^2) [1] occurs gradually which becomes well defined at 5 h and attains the maximum volume fraction of the crystalline phase. This is clearly evidenced from the observation of changes in XRD curves patterns as shown in (b) and (c) of Fig. 4. Thus accumulation of Li^+ ions in the phase-separated glass matrix initially could cause a slight increase of dielectric constant and with further heat-treatment time due to formation of stable $LiTaO_3$ ferroelectric crystals remarkably increase the dielectric constant reaching the highest value for 5 h heat-treated sample and then maintain almost same on further course of heat-treatment. The variation in the dielectric constant (ε_r) values among the heat-treated glass–ceramic nanocomposites are mostly due to volume fraction of crystal phases contained and also the dis-

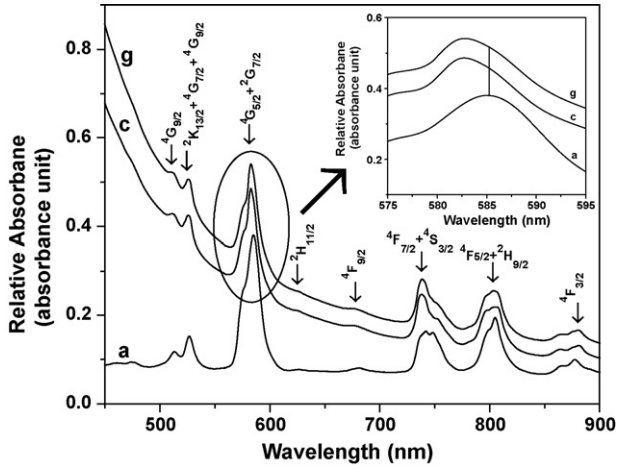

Fig. 10. Absorption spectra of samples a, c and g (thickness: 2 mm). Inset shows the peak position shifting of the hypersensitive transition, $^4I_{9/2} \rightarrow (^4G_{5/2}, {}^2G_{7/2})$, of Nd^{3+} ions in these samples in the wavelength range 575–595 nm.

tribution of the $LiTaO_3$ phase in the microstructure [38]. This result again ascertains the observations made from XRD and TEM analyses on the nanocrystallization of $LiTaO_3$ phase in the glass matrix.

3.6. UV–vis-NIR absorption spectra

The room temperature measured absorption spectra of the Nd^{3+}-doped precursor glass (a) and 5 and 100 h heat-treated glass–ceramic samples (c and g respectively) in the visible-NIR range have been presented in Fig. 10. The spectra reveal absorption peaks due to the $4f^3$–$4f^3$ forced electric dipole transitions from the ground $^4I_{9/2}$ state to different excited states of Nd^{3+} ion in $4f^3$ configuration. All the peaks $^4I_{9/2} \rightarrow {}^4G_{9/2}$ (512 nm), $^2K_{13/2} + {}^4G_{7/2} + {}^4G_{9/2}$ (526 nm), $^4G_{5/2} + {}^2G_{7/2}$ (583 nm), $^2H_{11/2}$ (626 nm), $^4F_{9/2}$ (679 nm), $^4F_{7/2} + {}^4S_{3/2}$ (739 nm), $^4F_{5/2} + {}^2H_{9/2}$ (806 nm) and $^4F_{3/2}$ (880 nm) are assigned in accordance with Carnall's convention [39,40]. From this figure it is noticed that the base line of absorption spectra of heat-treated samples ((c) and (g)) has been elevated significantly with the diminishing intensities of the absorption peaks. This uplifting can be attributed to scattering of short wavelength light by the crystals [41,42] or may be due to the difference in refractive index of crystalline phase (RI of $LiTaO_3$ is 2.1834 at 600 nm [30] with that of residual glassy matrix (RI = 1.7821 at 656.3 nm, see Table 1). Since the crystallites (14–36 nm) are smaller than the visible wavelength, a Rayleigh scattering model should be applicable [43]. According to this model, the scattering loss, τ is given by

$$\tau = \frac{32\pi^4 d^3 (n\Delta n)^2}{3\lambda^4} NV \quad (2)$$

where d is the particle diameter, λ the wavelength of light, n the refractive index, N the number density of particles, and V the volume of the particle. With progression of heat-treatment, the number and sizes of nanocrystallites developed in the glassy matrix increase and hence the scattering center and scattering loss increase that corresponds to a decrease in the visible transparency of the glass–ceramic nanocomposites. There is no significant difference in the shapes of absorption bands for glass and crystallized sample. During heat-treatment of the glasses, the hypersensitive transition $^4I_{9/2} \rightarrow {}^4G_{5/2}, {}^2G_{7/2}$ (obeying selection rule: $\Delta J \leq 2$, $\Delta L \leq 2$ and $\Delta S = 0$ with large value, 0.898 of squared reduced matrix element, $|U^{(2)}|^2$) of Nd^{3+} ion lying around 583 nm has been selected to understand the environment change closely around the rare-earth ion which is shown in Fig. 10 (inset). The spectrum is progressively sharpened in 100 h heat-treated sample (around 70 cm^{-1}) due to the line narrowing associated to the glass-crystal transformation around the rare-earth ion [44]. The band shift (around 70 cm^{-1} towards lower wavelength) is the sign for the transformation of environmental structure of Nd^{3+} site from amorphous to ordered crystalline, which confirms the incorporation of Nd^{3+} ions into $LiTaO_3$ crystallites during crystallization. The reason of band shifting towards lower wavelength can be well explained on the basis of covalent characteristics of hosts (glass and $LiTaO_3$ nanocrystals). The degree of covalent character of a host is estimated approximately using the formula [45]:

$$\text{Covalent character}\,(\%) = \exp[-0.25(\Delta\chi)^2] \times 100 \quad (3)$$

where $\Delta\chi$ is the electronegativity of the host, i.e. the electronegativity difference ($\chi_A - \chi_C$) of the anions and cations. The average electronegativity of anions (χ_A) or cations (χ_C) in the host is evaluated using simple additive relation [46]:

$$\chi_A \text{ or } \chi_C = \frac{\sum N_i \chi_i}{\sum N_i} \quad (4)$$

where N_i and χ_i are the number of individual constituent atom per mole and its electronegativity, respectively. The calculated covalent character of the precursor glass (LTSA) composition in this study is about 34% and $LiTaO_3$ nanocrystal is about 28%. As the degree of covalency is less in the $LiTaO_3$ nanocrystal host, so the absorption band shifts towards lower wavelength. This phenomenon is popularly known as the *"nephelauxetic effect"* after Jørgensen [47]. Similar correlation between the rare-earth band position shift and the degree of covalent character of various hosts has been established by Karmakar et al. [46,48,49].

3.7. NIR-excited NIR fluorescence and lifetime

The infrared fluorescence spectra (λ_{ex} = 809 nm) of the samples around 1069 nm are shown in Fig. 11. The emission band intensity around 1069 nm decreases with progression of heat-treatment. This decrease in emission intensity is due to the clustering of Nd^{3+} ions which is extremely sensitive to concentration quenching [50]. Dejneka [51] has demonstrated in fluoride glasses that clustering thereby quenching occurs when the Eu^{3+}–Eu^{3+} ionic separation is around 40 Å. In the present case, the Nd^{3+}–Nd^{3+} ionic separation (R_i)

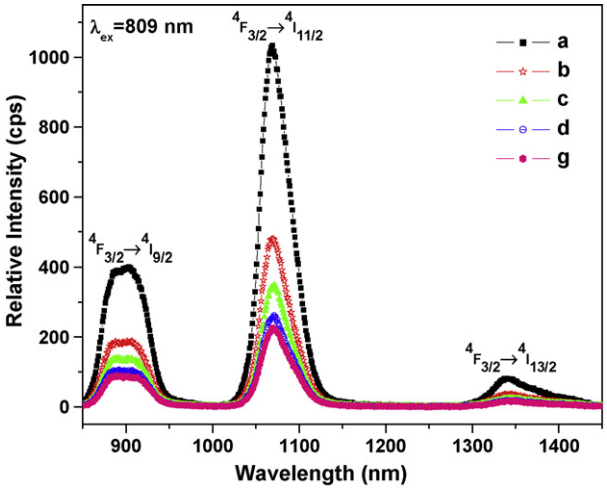

Fig. 11. Near infrared (NIR) fluorescence spectra (λ_{ex} = 809 nm) of Nd^{3+}:$LiTaO_3$ precursor glass and glass–ceramic nanocomposites obtained after heat-treatment for various duration ((a)–(d) and (g) indicate the sample identity). (For interpretation of the references to color in this figure legend, the reader is referred to the web version of the article.)

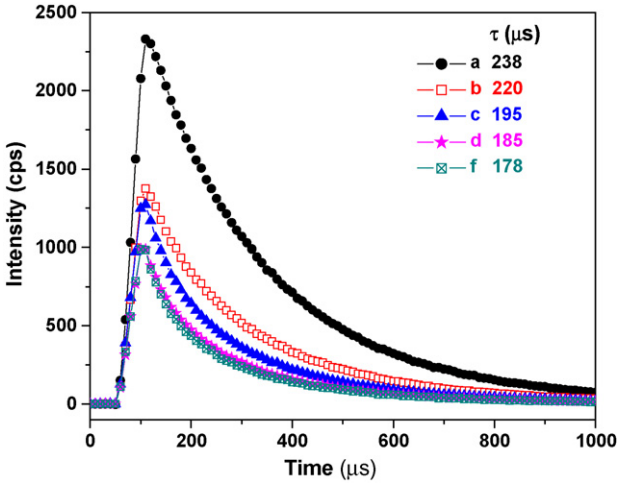

Fig. 12. Decay curves for the $^4F_{3/2} \rightarrow {}^4I_{11/2}$ transition of Nd^{3+} ion at 1069 nm under excitation at 809 nm of samples (a)–(d) and (f). (For interpretation of the references to color in this figure legend, the reader is referred to the web version of the article.)

in the precursor glass is found to be about 26 Å which was calculated using the relation [52]:

$$R_i(\text{Å}) = \left(\frac{1}{N_{Nd^{3+}}}\right)^{1/3} \quad (5)$$

where $N_{Nd^{3+}}$ is the Nd^{3+} ion concentration as already provided in Table 1. It is, therefore, seen that the Nd^{3+}–Nd^{3+} ionic separation (R_i) is in the quenching region. Theoretically, the rate of relaxation due to concentration quenching varies as R_i^{-6} [52–54]. With the progression of heat-treatment, the $LiTaO_3$ crystal phase has been formed and the Nd^{3+} ions partitioned into the residual glassy phase by reducing the inter-ionic separation less than 26 Å of precursor glasses. This fact results in reduction in fluorescence intensity (see curves (b)–(d) and (g), Fig. 11) due to concentration quenching. The emission bands become sharper and take shapes as in crystalline host with progress of heat-treatment duration. All these observations indicate that the Nd^{3+} ions enter into the $LiTaO_3$ crystalline phase and therefore, environment around Nd^{3+} ions is changed with progression of heat-treatment (see Section 3.6).

The room temperature fluorescence decay curves of the emission transition ($^4F_{3/2} \rightarrow {}^4I_{11/2}$) at 1069 nm with an excitation at 809 nm for Nd^{3+} ions in as-prepared glass and glass–ceramic nanocomposites have been depicted in Fig. 12. The measured curves demonstrate a single exponential decay. The excited state lifetime (τ) for all has been estimated from these decay curves and the results of samples (a)–(d) and (f) are shown in the inset of Fig. 12. It is seen that the excited state ($^4F_{3/2}$) lifetime (τ) decreases with increase in heat-treatment duration. This result indicates that Nd^{3+} ions undergoing clustering upon formation of glass-ceramics. This change in the heat-treatment conditions leads to changes in the volume of crystallinity in the glass-ceramics and in the lifetime of the $^4F_{3/2}$ state due to the concentration quenching [44,51]. Further investigations are in progress to examine the concentration effects and also the limiting concentration of the cluster formation in this host.

4. Conclusions

Transparent glass-ceramics containing $LiTaO_3$ nanocrystals in the aluminosilicate glass matrix were prepared and the formation of $LiTaO_3$ nanocrystals has been confirmed by XRD, FTIRR spectra, FESEM and TEM images. The nanocrystallite size of $LiTaO_3$ has been evaluated from XRD and found to vary in the range 14–36 nm. This evaluation correlates well with those obtained from TEM images. The increase of dielectric constant in comparison to precursor glass confirms the formation of high dielectric constant ferroelectric $LiTaO_3$ ($\varepsilon_r = 52$) in glassy matrix. The absorption spectra and NIR fluorescence spectra of glass–ceramic nanocomposites demonstrate that the Nd^{3+} ion has entered into the $LiTaO_3$ crystalline phase and form Nd^{3+}:$LiTaO_3$ nanocrystals. The decrease in NIR-excited emission intensity and fluorescence lifetimes with progression of heat-treatment time has been attributed to the clustering of Nd^{3+} ions which resulted in concentration quenching.

Acknowledgements

This research work was supported by BRNS/DAE under the sanction no. 2007/34/05-BRNS. The authors thank Dr. H.S. Maiti, Director, CGCRI for his keen interest and kind permission to publish this paper. Electron Microscope and X-Ray Divisions of CGCRI are also thankfully acknowledged.

References

[1] W.P. Risk, T.R. Gosnell, A.V. Nurmikko, Compact Blue-Green Lasers, Cambridge University Press, Cambridge, 2003.
[2] International Centre for Diffraction Data, JCPDS card file no. 29-0836.
[3] A.J. Moses, The Practicing Scientist's Handbook, Van Nostrand Reinhold Company, New York, 1978, p. 558.
[4] K.S. Abedin, T. Tsuritani, M. Sato, H. Ito, Appl. Phys. Lett. 70 (1997) 10.
[5] S. Zhu, Y. Zhu, Z. Yang, H. Wang, Z. Zhang, J. Hong, C. Ge, N. Ming, Appl. Phys. Lett. 67 (1995) 320.
[6] K. Mizuuchi, K. Yamamoto, Appl. Phys. Lett. 66 (1995) 2943.
[7] F. Zheng, H. Liu, D. Liu, S. Yao, T. Yan, J. Wang, J. Alloys Compd. 477 (2009) 688.
[8] Z.X. Cheng, H. Kimura, K. Ozawa, A. Miyazaki, C.V. Kanna, J. Alloys Compd. 402 (2005) 208.
[9] S. Youssef, R. Al Asmar, J. Podlecki, B. Sorli, A. Foucaran, Eur. Phys. J. Appl. Phys. 43 (2008) 65.
[10] I. Sokólska, J. Alloys Compd. 341 (2002) 288.
[11] I. Sokólska, S. Kück, G.D. Dzik, M. Baba, J. Alloys Compd. 323–324 (2001) 273.
[12] G. Gasparotto, S.A.M. Lima, M.R. Davolos, J.A. Varela, E. Longo, M.A. Zaghete, J. Lumin. 128 (2008) 1606.
[13] J.B. Gruber, T.H. Allik, D.K. Sardar, R.M. Yow, M. Scripsick, B. Wechsler, J. Lumin. 117 (2006) 233.
[14] H. Jain, Ferroelectrics 306 (2004) 111.
[15] W.R. Romanowski, I. Sokólska, G.D. Dzik, S. Gołab, J. Alloys Compd. 300–301 (2000) 152.
[16] H. Hase, H. Nasu, A. Mito, T. Hashimoto, J. Matsuoka, K. Kamiya, Jpn. J. Appl. Phys. 35 (1996) 5355.
[17] A. Tarafder, K. Annapurna, R.S. Chaliha, V.S. Tiwari, P.K. Gupta, B. Karmakar, J. Am. Ceram. Soc. 92 (2009) 1934.
[18] A. Tarafder, K. Annapurna, R.S. Chaliha, V.S. Tiwari, P.K. Gupta, B. Karmakar, J. Mater. Sci. 44 (2009) 4495.
[19] P. Mukherjee, K.B.R. Varma, Ferroelectrics 306 (2004) 129.
[20] S. Ito, T. Kokubo, M. Tashiro, J. Mater. Sci. 13 (1978) 930.
[21] P. Zeller, P. Peuser, Opt. Lett. 25 (2000) 34.
[22] F. Lahoz, I.R. Martín, U.R. Roríguez-Mendoza, I. Iparraguirre, J. Azkargorta, A. Mendioroz, R. Balda, J. Fernández, V. Lavín, Opt. Mater. 27 (2005) 1762.
[23] M.C. Silva, F.H. Cristovan, C.M. Nascimento, M.J.V. Bell, W.O. Cruz, A. Marletta, J. Non-Cryst. Solids 352 (2006) 5296.
[24] V. Seznec, H.L. Ma, X.H. Zhang, V. Nazabal, J.-L. Adam, X.S. Qiao, X.P. Fan, Opt. Mater. 29 (2006) 371.
[25] S. Mohan, K.S. Thind, G. Sharma, L. Gerward, Spectrochim. Acta A 70 (2008) 1173.
[26] S.J. Kim, J.E. Kim, Y.S. Yang, Ferroelectrics 272 (2002) 321.
[27] M.B. Volf, Chemical Approach to Glass, Elsevier, Amsterdam, 1984, p. 125.
[28] M. Yamane, Y. Asahara, Glasses for Photonics, Cambridge University Press, Cambridge, UK, 2000, p. 173.
[29] C. Hirayama, D. Berg, J. Am. Ceram. Soc. 46 (1963) 85.
[30] C.T. Lynch (Ed.), CRC Handbook of Materials Science, vol. III, CRC Press, Cleveland, Ohio, 1975, p. 170.
[31] J.Y. Hsu, R.F. Speyer, J. Am. Ceram. Soc. 72 (1989) 2334.
[32] B.D. Cullity, Elements of X-Ray Diffraction, 2nd ed., Addison-Wesley Publishing Co., London, 1978, p. 101.
[33] V.L. Burdick, D.E. Day, J. Am. Ceram. Soc. 50 (1967) 97.
[34] H. Ono, Y. Hosokawa, K. Shinoda, K. Koyanagi, H. Yamaguchi, Thin Solid Films 381 (2001) 57.
[35] J.Y. Zhang, I.W. Boyd, V. Dusastre, D.E. Williams, J. Phys. D: Appl. Phys. 32 (1999) L91–L95.
[36] A.J. Moulson, J.M. Herbert, Electroceramics: Materials. Properties. Applications, Chapman & Hall, London, 1990, p. 222.

[37] I.A. Blech, in: D.G. Fink, D. Christiansen (Eds.), Properties of Materials in Electronics Engineering Handbook, 2nd ed., McGraw-Hill, New York, 1986, pp. 6–30.
[38] D.E. Vernacotola, Key Eng. Mater. 94–95 (1994) 379–408.
[39] W.T. Carnall, P.R. Fields, K. Rajnak, J. Chem. Phys. 49 (1968) 4424.
[40] Y. Chen, Y. Huang, M. Huang, R. Chen, Z. Luo, J. Am. Ceram. Soc. 88 (2005) 19.
[41] G.H. Beall, D.A. Duke, in: D.R. Uhlmann, N.J. Kreidl (Eds.), Glass-Ceramic Technology in Glass Science and Technology, vol. 1, Academic Press, New York, 1983, p. 403.
[42] G.H. Beall, D.A. Duke, J. Mater. Sci. 4 (1969) 340.
[43] H.C. Van De Hulst, Light Scattering by Small Particles, Wiley, New York, 1957.
[44] M. Mortier, A. Monteville, G. Patriarche, G. Mazé, F. Auzel, Opt. Mater. 16 (2001) 255.
[45] L. Pauling, The Nature of Chemical Bond, 3rd ed., Cornell University Press, New York, 1970.
[46] B. Karmakar, J. Solid State Chem. 178 (2005) 2663.
[47] C.K. Jørgensen, Modern Aspects of Ligand Field Theory, North-Holland Publishing Co., Amsterdam, 1971.
[48] B. Karmakar, R.N. Dwivedi, J. Non-Cryst. Solids 342 (2004) 132.
[49] T. Som, B. Karmakar, J. Alloys Compd. 476 (2009) 383.
[50] P. Riello, S. Bucella, L. Zamengo, U. Anselmi-Tamburini, R. Francini, S. Pietrantoni, Z.A. Munir, J. Eur. Ceram. Soc. 26 (2006) 3301.
[51] M.J. Dejneka, J. Non-Cryst. Solids 239 (1998) 149.
[52] K. Pátek, Glass Lasers, Butterworth & Co. (Publishers) Ltd., London, 1970, p. 95.
[53] J.H. Campbell, T.I. Suratwala, J. Non-Cryst. Solids 263–264 (2000) 318.
[54] U. Kang, A.A. Zhilin, D.P. Logvinov, A.A. Onushchenko, V.A. Savost'yanov, T.I. Chuvaeva, A.V. Shashkin, Glass Phys. Chem. 27 (2001) 344.